collapse[16,23–25]. The rate at which energy is transferred out of the bubble is expected to increase as the thermal conductivity of the gas within the bubble increases. Bubbles containing helium, therefore, should be cooler than bubbles containing argon or xenon, although the predicted extent of this effect is debatable[24]. In order to examine the importance of thermal conduction, MBSL spectra were obtained from solutions of $Cr(CO)_6$ in octanol saturated with different noble gases. The results in Fig. 5 show that the temperature of MBSL decreases as the thermal conductivity of the gas within the bubble increases. Similar results were observed using dodecane.

We note that the thermal conductivities of the noble gases used here span a factor of thirty, while the thermal conductivities of the argon and hydrocarbon mixtures differ by only a factor of two, therefore, the temperature changes observed upon the addition of hydrocarbons to argon are not due to changes in thermal conductivity.

We have shown that the observed emission temperature within imploding cavitation bubbles depends on both the polytropic ratio and the thermal conductivity of the bubble contents. The processes occurring within the bubble, however, are more complex than can be described by the simple physics of compressional heating. A cavitation bubble functions as a small chemical reactor, and so the identity of the bubble contents will change during bubble collapse. The sonolysis of organic liquids generates H_2 and C_2H_2 as well as other small hydrocarbons[20], and similar processes will occur during the sonolysis of silicone oil. Evidence for this is seen in the MBSL spectra: the spectra of all the systems described here contain features attributable to excited states of C_2 and CH (refs 4, 18, 26), and we also find that sonication of silicone oil leads to intense emission from excited Si atoms. These chemical processes can absorb large amounts of energy during the compression. Furthermore, if sufficient dissociation occurs, the sonolysis products (mostly diatomics and polyatomics) will substantially lower the polytropic ratio and increase the pressure inside the bubble. This makes it increasingly difficult to further compress and heat the bubble[27]. These factors will limit the temperatures achievable by compressional heating within cavitation bubbles. □

Received 4 May; accepted 23 August 1999.

1. Suslick, K. S. & Crum, L. A. in *Handbook of Acoustics* (ed. Crocker, M. J.) 243–253 (Wiley-Interscience, New York, 1998).
2. Knapp, R. T., Daily, J. W. & Hammitt, F. G. *Cavitation* (McGraw-Hill, New York, 1970).
3. Barber, B. P. & Putterman, S. J. Observation of synchronous picosecond sonoluminescence. *Nature* **352,** 318–320 (1991).
4. Flint, E. B. & Suslick, K. S. The temperature of cavitation. *Science* **253,** 1325–1326 (1991).
5. Suslick, K. S., Hammerton, D. A. & Cline, R. E. Jr Sonochemical hot spot. *J. Am. Chem. Soc.* **108,** 5641–5642 (1986).
6. Suslick, K. S., Flint, E. B., Grinstaff, M. W. & Kemper, K. A. Sonoluminescence from metal carbonyls. *J. Phys. Chem.* **97,** 3098–3099 (1993).
7. Alkemande, C. T. J., Hollander, T., Snelleman, W. & Zeegers, P. J. T. *Metal Vapours in Flames* (Pergamon, New York, 1982).
8. Wiese, W. L., Fuhr, J. R. & Martin, G. A. Atomic transition probabilities: scandium through manganese. *J. Phys. Chem. Ref. Data* **17,** 311–327 (1988).
9. Wiese, W. L., Fuhr, J. R. & Martin, G. A. Atomic transition probabilities: iron through nickel. *J. Phys. Chem. Ref. Data* **14,** 13–67 (1988).
10. Whaling, W. & Brault, J. W. Comprehensive transition probabilities in molybdenum I. *Phys. Scr.* **38,** 707–715 (1988).
11. Gaydon, A. G. *The Spectroscopy of Flames* 2nd edn (Wiley, New York, 1974).
12. Cabannes, F. & Chapelle, J. in *Reactions Under Plasma Conditions* 1st edn Vol. 1 (ed. Venugopalan, M.) 367–470 (Wiley-Interscience, New York, 1971).
13. Reif, I., Fassel, V. A. & Kniseley, R. N. Spectroscopic flame measurements and their physical significance I: theoretical concepts. *Spectrochim. Acta B* **28,** 105–123 (1973).
14. Jeffries, J. B., Copeland, R. A., Suslick, K. S. & Flint, E. B. Thermal equilibration during cavitation. *Science* **256,** 248 (1992).
15. Noltingk, B. E. & Neppiras, E. Cavitation produced by ultrasonics. *Proc. Phys. Soc. B* **63,** 674–685 (1950).
16. Kamath, V., Prosperetti, A. & Egolfopoulos, F. N. A theoretical study of sonoluminescence. *J. Acoust. Soc. Am.* **94,** 248–260 (1993).
17. Jarman, P. Measurements of sonoluminescence from pure liquids and some aqueous solutions. *Proc. Phys. Soc.* **73,** 628–640 (1959).
18. Flint, E. B. & Suslick, K. S. Sonoluminescence from nonaqueous liquids: emissions from small molecules. *J. Am. Chem. Soc.* **111,** 6987–6992 (1989).
19. Suslick, K. S. & Flint, E. B. Sonoluminescence of alkali metal salts. *J. Phys. Chem.* **95,** 1484–1488 (1991).
20. Suslick, K. S., Gawienowski, J. J., Schubert, P. F. & Wang, H. H. Alkane sonochemistry. *J. Phys. Chem.* **87,** 2299–2301 (1983).
21. Suslick, K. S., Gawienowski, J. W., Schubert, P. F. & Wang, H. H. Sonochemistry in non-aqueous liquids. *Ultrasonics* **22,** 33–36 (1984).
22. Yaws, C. L. *Handbook of Vapor Pressures* Vol. 3, 383 (Gulf, Houston, 1994).
23. Hickling, R. Effects of thermal conduction in sonoluminescence. *J. Acoust. Soc. Am.* **35,** 967–974 (1963).
24. Young, F. R. Sonoluminescence from water containing dissolved gases. *J. Acoust. Soc. Am.* **60,** 100–104 (1976).
25. Yasui, K. *J. Phys. Soc. Jpn* **65,** 2830–2840 (1996).
26. Suslick, K. S. & Flint, E. B. Sonoluminescence of non-aqueous liquids. *Nature* **330,** 553–555 (1987).
27. Zel'dovich, Y. D. & Raizer, Y. P. *Physics of Shock Waves and High Temperature Hydrodynamic Phenomenon* 2nd edn (Academic, New York, 1966).

Acknowledgements

This work was supported by the US National Science Foundation, the US Department of Energy, and in part by the US Defence Advanced Research Projects Agency.

Correspondence and requests for materials should be addressed to K.S.S. (e-mail: ksuslick@uiuc.edu).

Carbon cycling and chronology of climate warming during the Palaeocene/Eocene transition

Richard D Norris* & Ursula Röhl†

* *MS-23, Woods Hole Oceanographic Institution, Woods Hole, Massachusetts 02540-1541, USA*

† *Fachbereich Geowissenschaften, Universität Bremen, Postfach 330 440, 28334 Bremen, Germany*

Current models of the global carbon cycle lack natural mechanisms to explain known large, transient shifts in past records of the stable carbon-isotope ratio ($\delta^{13}C$) of carbon reservoirs[1,2]. The injection into the atmosphere of ~1,200–2,000 gigatons of carbon, as methane from the decomposition of sedimentary methane hydrates, has been proposed to explain a $\delta^{13}C$ anomaly[3,4] associated with high-latitude warming[1] and changes in marine[5–7] and terrestrial[8] biota near the Palaeocene–Eocene boundary, about 55 million years ago. These events may thus be considered as a natural 'experiment' on the effects of transient greenhouse warming. Here we use physical, chemical and spectral analyses of a sediment core from the western North Atlantic Ocean to show that two-thirds of the carbon-isotope anomaly occurred within no more than a few thousand years, indicating that carbon was catastrophically released into the ocean and atmosphere. Both the $\delta^{13}C$ anomaly and biotic changes began between 54.93 and 54.98 million years ago, and are synchronous in oceans and on land. The longevity of the $\delta^{13}C$ anomaly suggests that the residence time of carbon in the Palaeocene global carbon cycle was ~120 thousand years, which is similar to the modelled response after a massive input of methane[3,4]. Our results suggest that large natural perturbations to the global carbon cycle have occurred in the past—probably by abrupt failure of sedimentary carbon reservoirs—at rates that are similar to those induced today by human activity.

The carbon isotope record of marine carbonates is interrupted by a transient negative $\delta^{13}C$ anomaly of −3‰ over an interval of ~100–200 kyr near the end of the Palaeocene[1,9–13]. In the oceans, the $\delta^{13}C$ anomaly is associated with the extinction of 35–50% of cosmopolitan benthic foraminifera[7,10], the appearance of three short-ranging planktic foraminifera[5], a widespread increase in

kaolinite (interpreted to herald a warm, wet climate), and a dramatic warming of high-latitude surface water and deep water (by ~5–7 °C) (ref. 1). The benthic foraminifer extinction and the rise in temperatures have been interpreted as indications of greenhouse warming and formation of oxygen-deficient deep waters[1]. A $\delta^{13}C$ anomaly has also been observed in terrestrial soil carbonates and mammal teeth associated with a major turnover in land mammal assemblages[8,14–16]. However, uncertainties in the number[9] and correlation of the $\delta^{13}C$ events have led to estimates of their age ranging from 54.88 to 55.5 Myr (refs 8, 17–20). Here, we explore the age and duration of the $\delta^{13}C$ event using an astronomically calibrated timescale.

The Ocean Drilling Program (ODP) Site 1051 on Blake Nose in the western North Atlantic preserves an apparently unbroken record of magnetochron C24r and the events surrounding the Palaeocene–Eocene boundary[21]. In all, the record of chron C24r spans ~76 m of siliceous nannofossil chalk at ODP Site 1051, making this the thickest known sedimentary record of this magnetochron in the deep sea. We analysed records of iron (Fe) intensities (counts per second), measured by a non-destructive X-ray fluorescence (XRF) core scanner[17,22], and magnetic susceptibility (Fig. 1).

The benthic foraminifer extinction[10] occurs at 512.80 m.c.d. (metres composite depth) in ODP Site 1051 and is closely associated with the first-appearance datum of the calcareous nannofossil *Rhomboaster cuspis* that marks the base of biozone CP9a (ref. 21). Planktonic foraminifera characteristic of the $\delta^{13}C$ event (*Morozovella allisonensis*, *Acarinina sibiayaensis*, and *Acarinina africana*) appear over an interval, 3 m thick, immediately above the benthic extinction horizon (Fig. 2). These biostratigraphic events occur near the middle of planktic foraminifer biozone P5, in agreement with other deep-sea sites[5,20], and verify that ODP Site 1051 is representative of the deep-sea record. Stable-isotope analyses of bulk carbonate from ODP Site 1051 demonstrate that the benthic foraminifer extinction and associated biostratigraphic events coincide with a ~1.6‰ $\delta^{13}C$ excursion (Fig. 2). Analyses of the planktic foraminifer *Morozovella subbotinae* show a 2.8‰ $\delta^{13}C$ decrease through the carbon isotope anomaly, which suggests that Site 1051 records the full magnitude of the excursion. The $\delta^{13}C$ anomaly in bulk carbonate records the sharp initial drop and more gradual recovery typical of correlative events in other deep sea sites, such as ODP Site 690 in the Southern Ocean[1,2] and ODP Site 1001 in the Caribbean[13].

Colour reflectance[21], magnetic susceptibility, and Fe intensity data from ODP Site 1051 display well defined cycles throughout the upper Palaeocene (Fig. 1). Counts of Fe-intensity cycles reveal 23–25 cycles with chron C25n at ODP Site 1051. The uncertainty in the cycle count is due to a gap of 70 cm in discrete magnetic polarity measurements at the top of chron C25n. The estimated duration of chron C25n is ~487 kyr (ref. 20) which suggests that the Fe-intensity cycles are each 20–21 kyr long. The cycle duration is remarkably close to the modern mean precession period of ~21 kyr (ref. 23) that is the average of the 23- and 19-kyr precession bands.

Spectral analysis of the Fe intensity between 516 to 526 m.c.d. displays strong spectral power at wavelengths of 23 cm and 29 cm. The ratios of the Fe-intensity spectral peaks and their relative magnitudes are similar to those of the characteristic double peaks for the 19- and 23-kyr cycles in modern insolation spectra for the same latitude as Site 1051 (Fig. 3a and b). The Fe-intensity and magnetic-susceptibility cycles are probably due to variations in

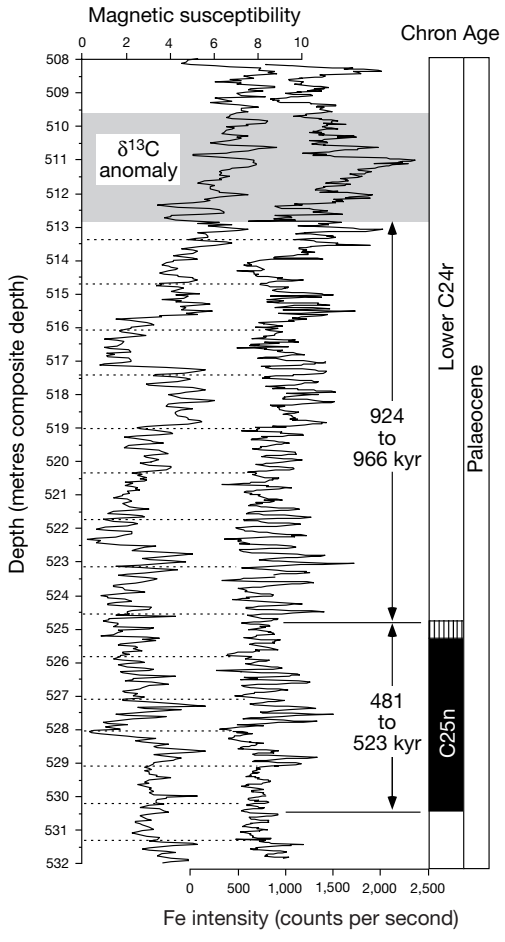

Figure 1 Cyclostratigraphy and magnetochronology of the uppermost Palaeocene. Magnetic susceptibility, Fe intensity and magnetostratigraphy from ODP Site 1051 on the Blake Nose (30° 03′ N; 75° 21′ W, 1,983 m water depth). Ages are estimated from counts of physical property cycles and assumption of a duration of 21 kyr per cycle (see Fig. 3). Horizontal dashed lines bundle groups of five cycles. The depth scale is based on a spliced record of magnetic susceptibility and Fe intensity in holes 1051A and 1051B. The resulting composite record was cross-checked with downhole logging[21] of magnetic susceptibility and FMS (formation microscanner) resistivity. The position of the $\delta^{13}C$ anomaly (Fig. 2) is shown as a shaded band. Post-cruise analysis of discrete samples demonstrate the existence of normal-polarity events in ODP Hole 1051A which have been confirmed as chrons C25n and C24n based on planktic foraminifera and calcareous nannofossil biostratigraphy as well as by correlation of downhole logs to the magnetic polarity record from nearby ODP Site 1050 (ref. 21). Uncertainty in the placement of the top of normal polarity chron C25n is shown by a striped band. The base of C25n is based upon shipboard pass-through magnetometer results[21].

carbonate productivity and iron input from terrestrial sources, but may also reflect variations in carbonate dissolution.

Our cyclostratigraphy provides, to our knowledge, the first astronomically calibrated duration for the $\delta^{13}C$ anomaly. The primary-cycle wavelength increases from 23–29 cm below the $\delta^{13}C$ anomaly to ~51 cm within it, and increases again to ~105 cm above it (Fig. 3a). These power spectra maintain a double-peaked pattern above and below the $\delta^{13}C$ anomaly that we interpret as representing the main precession bands. The precession cycles seem to have been attenuated by a large increase in sedimentation rate above ~513 m.c.d. There appear to be a total of 7 magnetic susceptibility cycles between the onset of the anomaly and the point at which $\delta^{13}C$ reaches the post-anomaly average ratio (~509.8 m.c.d.; Fig. 2). The entire excursion thus lasted ~150 kyr.

Our estimate for the duration of the excursion has an error of ±1.7 kyr, associated with the assumption of a 21-kyr average for seven precession cycles[23] and potentially larger errors associated with our identification of the start and end of the $\delta^{13}C$ anomaly. A debris flow of chalk clasts[21] occurs just below the $\delta^{13}C$ anomaly and may have eroded several thousand years of sedimentation. In addition, we have chosen the termination of the $\delta^{13}C$ anomaly to be near its asymptote with post-excursion ratios, but a small shift in this level could change the duration of the anomaly by ~20 kyr or more.

Cycle counting demonstrates that the initial release of ^{12}C was very fast, and continued over an extended period. There is ~1 cycle between the base of the excursion and the point at which minimum $\delta^{13}C$ ratios are reached and a total of 1.5 cycles between the start of the event and the point at which $\delta^{13}C$ begins to rise again. The $\delta^{13}C$ of bulk carbonate drops abruptly from 2.2‰ to 0.96‰ at the start of the event and decreases more slowly over the next ~20 kyr before reaching near-minimum ratios of ~0.58‰. Minimum $\delta^{13}C$ levels are maintained for as much as an additional 10 kyr. Our results are similar to isotopic measurements of benthic foraminifera and bulk carbonate from ODP Hole 690B that show a sharp drop in $\delta^{13}C$ followed by a more gradual shift to minimum $\delta^{13}C$ (refs 1, 2) levels.

The cyclostratigraphy suggests that about two-thirds of the $\delta^{13}C$ shift was completed catastrophically within a few thousand years or less. Given the large mass of carbon in the global carbon cycle (~42,000 Gton, ref. 3) it is hard to perturb the carbon-isotope composition of the oceans and atmosphere without a massive injection of isotopically light carbon, such as bacterial methane[3,4]. Hence, our data strongly supports models for abrupt release of methane from submarine reservoirs by slope failure[2–4]. The extended period taken to reach minimum $\delta^{13}C$ suggests that methane, or another source of ^{12}C, bled into the oceans and atmosphere over ~30 kyr at a rate more than sufficient to balance its removal by burial. Gradual venting of ^{12}C-enriched material may reflect the time required to destabilize methane reservoirs in successively deeper waters through a feedback process. We suggest that the feedback system involved CO_2-induced greenhouse warming of deep waters at their sites of formation followed by the collapse of additional hydrate reservoirs by hydrate melting and slope failure under warm deep water[2–4]. Any feedback between global warming and carbon release must have stopped about 30 kyr after it began, at

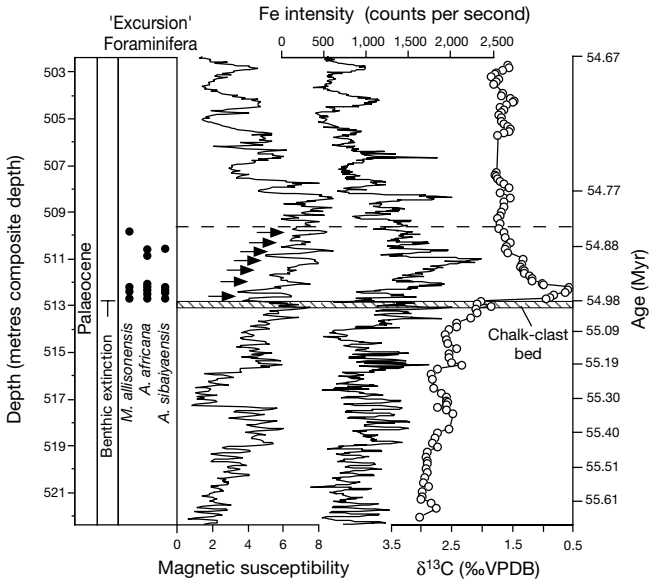

Figure 2 Stratigraphy around the $\delta^{13}C$ anomaly. Left to right: ranges of members of the 'excursion fauna' of planktic foraminifera (see text), magnetic susceptibility, Fe intensity, and $\delta^{13}C$ of bulk carbonate in ODP Site 1051. Small arrows show approximate positions of peaks in magnetic-susceptibility and Fe-intensity cycles believed to represent ~21-kyr precession cycles within the $\delta^{13}C$ anomaly. The dashed line shows the position of the termination of the $\delta^{13}C$ anomaly, and the hatched bar shows the position of the chalk-clast horizon. The age scale is based upon the locations of minima in magnetic susceptibility assuming an age of 54.98 Myr for the base of the $\delta^{13}C$ anomaly. Note the attenuation of the age scale due to an increase in sedimentation rate above the chalk-clast horizon. VPDB, Vienna Pee Dee Belemnite.

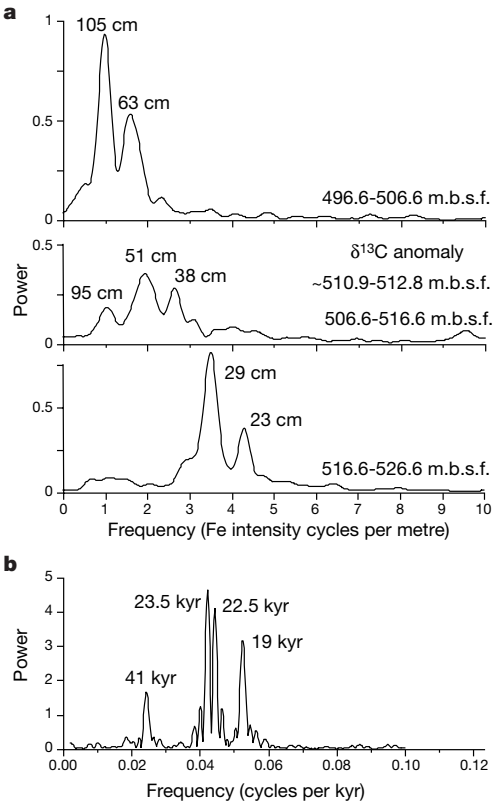

Figure 3 Power spectra for Site 1051 and modern summer insolation. **a**, Power spectra are shown for three 10-m windows in Site 1051. The double peak in spectra for 499.6–506.6 and 516.6–526.6 metres composite depth (m.c.d.) strongly suggests that the major cycles in the Fe-intensity and magnetic-susceptibility records reflect the 19- and 23-kyr precession bands. The increase in wavelength of the major Fe-intensity cycles suggests an increase in sedimentation rate within and above the $\delta^{13}C$ anomaly. The peak in spectral power at 95 cm in the 506.6–516.6 m.c.d. spectrum reflects the rapid shift from a dominant 51-cm cycle to an ~1-m cycle within this 10-m-thick interval. Power–depth spectra were created using the Blackman–Tukey method on 50-point detrended Fe-intensity records (Fig. 1). **b**, Power spectra for the modern summer insolation at 30° N. Modern insolation was calculated using the method of Berger[29]. All spectra were generated with the Analyseries software package[30]. m.b.s.f., metres below sea floor.

which point $\delta^{13}C$ began its exponential rise toward the average post-excursion ratios.

There are 44–46 magnetic-susceptibility and Fe-intensity cycles of wavelength ~23–29 cm between the top of chron C25n and the beginning of the $\delta^{13}C$ anomaly at Site 1051 (Fig. 1). The cycle count suggests that the $\delta^{13}C$ anomaly began 924–966 kyr after the end of chron C25n. Cande and Kent[24] estimate an age of 55.9 Myr for the top of chron C25n, which places the start of the $\delta^{13}C$ anomaly at 54.93–54.98 Myr. These dates for the $\delta^{13}C$ anomaly are maximum ages, as some sediment may have been eroded during deposition of the chalk clast layer.

The 55.9 Myr data for the top of chron C25n may be significantly in error. The date is based on the calibration point of 55 Myr for the calcareous nannofossil zone NP9/NP10 boundary[18,24] which, unfortunately, was established where the zonal boundary is an unconformity[18]. This 55-Myr date was used[29] to estimate the ages of the C24n and C25n polarity boundaries. As the NP9/N10 boundary is known to be younger than the $\delta^{13}C$ anomaly[18,20], the two events cannot have the same age and the 55.9-Myr age for the top of chron C25n must therefore be inaccurate. Accordingly, our absolute ages for events around the $\delta^{13}C$ anomaly will need to be revised when the ages of the magnetochrons are determined more precisely.

Our dates of ~54.93–54.98 Myr for the $\delta^{13}C$ anomaly and the associated climatic and biotic events show that these are synchronous with a $\delta^{13}C$ anomaly and biotic changes on land. A date of 54.96 Myr has been estimated for the prominent $\delta^{13}C$ excursion and the Wasatchian 0 provincial land-mammal age in the Bighorn basin, Wyoming, based on calculated sedimentation rates between the top of C25n (55.9 Myr) and the base of C24n (53.35 Myr) (ref. 25). Both the Bighorn-basin chronology and our chronology for Site 1051 are based on the same estimated ages[24] for the magnetic polarity events. We conclude that the age of the $\delta^{13}C$ anomaly relative to the top of chron C25n is easily within the same age range in the marine and terrestrial records, contrary to previous dates for the marine $\delta^{13}C$ event[18,20].

The synchroneity of the $\delta^{13}C$ event in the ocean and atmosphere unites the immigration of mammals such as artiodactyls, perissodactyls and primates into North America[8,26,27] with the warming of subtropical and high-latitude oceans and the development of widespread disaerobic conditions in the deep sea[7,10]. The initial release of ^{12}C-enriched carbon occurred over no more than a few thousand years and is precisely coincident with the benthic foraminifer extinction and the origination of the "excursion fauna" of planktic foraminifera.

The Site 1051 cyclostratigraphy shows that the entire $\delta^{13}C$ anomaly occurred over a span of ~150 ± 20 kyr. The $\delta^{13}C$ anomaly developed over ~30 kyr, whereas the carbon released during the initial phases of the excursion was sequestered by burial over the remaining ~120 kyr. Therefore, the residence time of carbon in the global carbon cycle was ~120 kyr in the Palaeocene. Our estimate of the time to sequester carbon by burial will need to be confirmed at other sites; however, it agrees with the calculated modern carbon residence time of 140 kyr after injection of 1,200 Gton of methane into the pre-industrial carbon cycle[3,4]. We suggest that the rate of carbon cycling was not very different from today during warm times such as the Palaeocene and early Eocene.

Current carbon-cycle models do not explicitly include exchange fluxes for methane hydrates and other deeply buried carbon sources other than by anthropogenic release[4]. Yet modern oceanic hydrate reservoirs contain more than 14,000 Gton of methane[28], which is large compared to the remaining total exchangeable carbon reservoir (~42,000 Gton, ref. 3). The size of the Palaeocene–Eocene carbon-isotope excursion and the rapidity of its onset demonstrates that there must be a large reservoir of exchangeable carbon that can be released by natural processes on timescales similar to modern rates of anthropogenic carbon input. □

Received 3 May; accepted 14 September 1999.

1. Kennett, J. P. & Stott, L. D. Abrupt deep-sea warming, paleoceanographic changes and benthic extinctions at the end of the Paleocene. *Nature* **353,** 225–229 (1991).
2. Bains, S., Corfield, R. M. & Norris, R. D. Mechanisms of climate warming at the end of the Paleocene. *Science* **285,** 724–727 (1999).
3. Dickens, G. R., O'Neil, R. R., Rea, D. K. & Owen, R. M. Dissociation of oceanic methane hydrate as a cause of the carbon isotope excursion at the end of the Paleocene. *Paleoceanography* **10,** 965–971 (1995).
4. Dickens, G. R. Methane oxidation during the late Paleocene thermal maximum. *Bull. Soc. Géol. Fr.* (in the press).
5. Kelly, D. C., Bralower, T. J., Zachos, J. C., Permoli Silva, I. & Thomas, E. Rapid diversification of planktonic foraminifera in the topical Pacific (ODP Site 865) during the late Paleocene thermal maximum. *Geology* **24,** 423–426 (1996).
6. Thomas, E. in *Global Catastrophies in Earth History: an Interdisciplinary Conference on Impacts, Volcanism, and Mass Mortality* (eds Sharpton, V. L. & Ward, P.) 481–495 (Geological Society of America, Boulder, Colorado, 1990).
7. Thomas, E. in *Late Paleocene-Early Eocene Climatic and Biotic Events* (eds Aubry, M.-P., Lucas, S. & Berggren, W. A.) 214–243 (Colombia Univ. Press, New York, 1998).
8. Koch, P. L., Zachos, J. C. & Gingerich, P. D. Correlation between isotope records in marine and continental carbon reservoirs near the Palaeocene/Eocene boundary. *Nature* **359,** 319–322 (1992).
9. Stott, L. D., Kennett, J. P., Shackleton, N. J. & Corfield, R. M. The evolution of Antarctic surface waters during the Paleogene: inferences from stable isotopic composition of planktonic foraminifera. *Proc. ODP Sci. Res.* **113,** 849–863 (1990).
10. Thomas, E. & Shackleton, N. J. in *Correlation of the Early Paleogene in Northwest Europe* (eds Knox, R. W., Corfield, R. M. & Dunay, R. E.) 401–441 (Geological Society, London, 1996).
11. Pak, D., Miller, K. G. & Browning, J. Global significance of an isotopic record from the New Jersey Coastal Plain: Linkage between the shelf and deep sea in the late Paleocene to early Eocene. *Proc. ODP Sci. Res. X* **150,** 305–315 (1997).
12. Lu, G. & Keller, G. (1993). The Palaeocene-Eocene transition in the Antarctic Indian Ocean: Inference from planktonic foraminifera. *Mar. Micropaleontol.* **21,** 101–142 (1993).
13. Bralower, T. J. *et al.* High resolution records of the late Paleocene thermal maximum and circum-Caribbean volcanism: is there a causal link? *Geology* **25,** 963–966 (1997).
14. Koch, P. L., Zachos, J. C. & Dettman, D. L. Stable isotope stratigraphy and paleoclimatology of the Paleogene Bighorn Basin (Wyoming, USA). *Palaeogeogr., Palaeoclimatol., Palaeoecol.* **115,** 61–89 (1995).
15. Clyde, W. C. & Gingerich, P. D. Mammalian community response to the latest Palaeocene thermal maximum: An isotaphonomic study in the northern Bighord Basin, Wyoming. *Geology* **26,** 1011–1014 (1998).
16. Hooker, J. J. in *Late Paleocene-Early Eocene Climatic and Biotic Events* (eds Aubry, M.-P., Lucas, S. & Berggren, W. A.) 428–450 (Columbia Univ. Press, New York, 1998).
17. Röhl, U. & Abrams, L. J. in *Proc. ODP Sci. Res.* (eds Leckie, R. M. *et al.*) Vol. 165 (Ocean Drilling Program, College Station, Texas, in the press).
18. Aubry, M.-P., Berggren, W. A., Stott, L. D. & Sinha, A. in *Correlation of the Early Paleogene in Northwest Europe* (eds Knox, R. W., Corfield, R. M. & Dunay, R. E.) 353–380 (Geological Society, London, 1996).
19. Wing, S. L. in *Late Paleocene-Early Eocene Climatic and Biotic Events* (eds Aubry, M.-P., Lucas, S. & Berggren, W. A.) 380–400 (Columbia Univ. Press, New York, 1998).
20. Berggren, W. A., Kent, D. V., Swisher, C. C. III & Aubry, M.-P. in *Geochronology, Time Scales and Global Stratigraphic Correlations: A Unified Temporal Framework for an Historical Geology* (eds Berggren, W. A., Kent, D. V., Aubry, M.-P. & Hardenbol, J.) 129–212 (Society for Economic Paleontologists and Mineralogists, Tulsa, Oklahoma, 1995).
21. Norris, R. D. *et al.* Black Nose Paleoceanographic Transect, Western North Atlantic. *Proc. ODP Init. Rep. B* **171,** 1–749 (1998).
22. Jansen, J. H. F., Van der Gaast, S. J., Koster, B. & Vaars, A. J. CORTEX, a shipboard XRF-scanner for element analyses in split sediment cores. *Mar. Geol.* **151,** 143–153 (1998).
23. Herbert, T. D., Premoli Silva, I., Erba, E. & Fischer, A. G. in *Geochronology, Time Scales and Global Stratigraphic Correlation* (eds Berggren, W. A., Kent, D. V., Aubry, M.-P. & Hardenbol, J.) 81–93 (Society for Economic Paleontologists and Mineralogists, Tulsa, Oklahoma, 1995).
24. Cande, S. C. & Kent, D. V. Revised calibration of the geomagnetic polarity time scale for the Late Cretaceous and Cenozoic. *J. Geophys. Res.* **100,** 6093–6095 (1995).
25. Wing, S. L., Boa, H. & Koch, P. L. in *Warm Climates in Earth History* (eds Huber, B. T., MacLeod, K. & Wong, S. L.) (Cambridge Univ. Press, Cambridge, UK, in the press).
26. Wing, S. L., Alroy, J. & Hickey, L. J. Plant and mammal diversity in the Paleocene to early Eocene of the Bighorn Basin. *Palaeogeogr., Palaeoclimatol., Palaeoecol.* **115,** 117–155 (1995).
27. Maas, M., Anthony, M. R. L., Gingerich, P. D., Gunnell, G. F. & Krause, D. W. Mammalian genetic diversity and turnover in the Late Paleocene and early Eocene of the Bighorn and Crazy Mountains Basins, Wyoming and Montana (USA). *Palaegeogr., Palaeoclimatol., Palaeoecol.* **115,** 181–207 (1995).
28. Gornitz, V. & Fung, I. Potential distribution of methane hydrates in the world's oceans. *Glob. Biogeochem. Cycles* **8,** 335–347 (1994).
29. Berger, A. Long-term variations of daily insolation and quaternary climatic change. *J. Atmos. Sci.* **35,** 2362–2367 (1978).
30. Paillard, D., Labeyrie, L. & Yiou, P. Macintosh program performs time-series analysis. *Eos* **77,** 379 (1996).

Acknowledgements

We thank G. Dickens, M. P. Aubry, W. A. Berggren, D. Kent, P. Koch and D. Kroon for discussions, and the staff of the Ocean Drilling Program in Bremen for technical assistance. This work was supported by the Joint Oceanographic Institutions—US Science Support Advisory Committee (JOI-USSAC), and the National Science Foundation and the Deutsche Forhungsgemeinschaft.

Correspondence and requests for materials should be addressed to R.D.N. (e-mail: rnorris@whoi.edu).